Title

Vibrational correlation between conjugated carbonyl and diazo modes studied by single- and dual-frequency two-dimensional infrared spectroscopy

Authors

Maekawa, Hiroaki
Sul, Soohwan
Ge, Nien-Hui

Publication Date

2013-08-01

DOI

10.1016/j.chemphys.2013.02.010

Peer reviewed

Published in Chemical Physics 422:22-30 Aug 2013

Vibrational Correlation between Conjugated Carbonyl and Diazo Modes Studied by Single and Dual Frequency Two-Dimensional Infrared Spectroscopy

Hiroaki Maekawa, Soohwan Sul,[†] and Nien-Hui Ge*

Department of Chemistry, University of California at Irvine, Irvine, California, 92697-2025

* To whom correspondence should be addressed.

Email address: nhge@uci.edu. Phone: 949-824-1263. FAX: 949-824-8571

[†] Present address: Center for Computer Simulation and Analytical Science, Samsung Advanced Institute of Technology, Yongin 446-712, Republic of Korea

Abstract

We have applied infrared three-pulse photon echo and single- and dual-frequency 2D IR spectroscopy to the ester C=O and diazo N=N stretching modes in ethyl diazoacetate (EDA), and investigated their vibrational frequency fluctuations and correlation. The two modes exhibit different vibrational dynamics and 2D lineshape, which are well simulated by frequency-frequency correlation functions (FFCFs) with two decaying components. Although the FTIR spectrum shows a single C=O band, absolute magnitude 2D IR nonrephasing spectrum displays spectral signatures supporting the presence of *cis* and *trans* conformations. The cross-peak inclined toward the anti-diagonal in the dual-frequency 2D IR spectrum, indicating that the frequency fluctuations of the two modes are anticorrelated. This behavior is attributed to anticorrelated change in the bond orders when solvent and structural fluctuations causes EDA to adopt a different mixture of the two dominant resonance structures. The effects of cross FFCF on the cross-peak line shape are discussed.

Keywords

Two-dimensional infrared spectroscopy, Nonlinear infrared spectroscopy, Frequency-frequency correlation function, Diazo ester

1. Introduction

Since the development of coherent two-dimensional infrared (2D IR) spectroscopy more than ten years ago,[1] this powerful technique has revealed new structural and dynamic information in condensed phase systems through detailed measurements of vibrational couplings and dynamics.[2-9] Much of the information is hardly available from conventional techniques. For example, vibrational coupling is a major factor that governs 2D IR cross-peak patterns. Since the coupling depends on the geometrical configuration of vibrational modes, they can be directly related to structure. Many experimental and theoretical studies have shown that amide-I 2D IR spectra are very useful for elucidating structures of biological macromolecules.[2,5,10] Another example is to directly probe ultrafast chemical exchange processes through waiting-time dependent 2D IR.[7,11-15] In this work, we will focus on vibrational frequency correlation.

Frequency correlation between different vibrational modes, e.g., whether their frequencies fluctuate randomly or in a concerted way, is a subject of great interest but hard to access experimentally before 2D IR techniques became available.[16-22] It is well known that vibrational frequency is sensitive to the chemical environment around an oscillator, such as hydrogen bonds, ligand binding, and substituent effects.[23] However, it was not until 10-15 years ago that researchers started to have the means to measure the time scales and amplitudes of vibrational frequency fluctuations and from which to gain understanding on molecular dynamics in solutions and proteins.[24-30] Knowledge on how different vibrational modes correlate with one another can provide us with a new microscopic view to study molecules in the condensed phases. Coherent 2D IR spectroscopy is the only technique that can directly probe intra- and intermolecular frequency correlations. It should be noted that the concept of correlation here is completely different from that of 2D IR correlation spectroscopy developed by Noda,[31,32] which probes correlative changes of IR intensity signals induced by external perturbation, such as pressure, temperature, etc.

Measuring frequency correlation between vibrational modes of very different frequencies using coherent 2D IR spectroscopy is a technical challenge. Because the typical spectral width of a femtosecond IR pulse is 150–300 cm^{-1}, it covers less than 10% of the spectral range of high-frequency vibrational modes (1000–4000 cm^{-1}). Single-color 2D IR method is not applicable to measure the correlation, for example, between the O–H stretching and H–O–H bending modes of water. To circumvent this problem, one needs to use dual-frequency 2D IR spectroscopy[18-22,33,34] in which two mid-IR sources can be tuned independently to excite distinct modes. Due to technical difficulties only a few groups conducted dual-frequency 2D IR measurements so far. Hochstrasser and coworkers applied the dual-frequency technique to measure coupling strengths and correlation between the amide-I and amide-II of *N*-

methylacetamide (NMA),[18] the amide-I and amide-A of model peptides[19], and the N–H and C=O stretchings of a molecular complex formed by an intermolecular hydrogen bond.[20] Rubtsov and coworkers measured dual-frequency 2D IR spectra of numerous compounds and mode pairs[35], for example, the C=O and C≡N modes in 2-cyanocoumarin,[21] and the C-D and C≡N modes in acetonitrile-d_3.[22] Other interesting studies using dual frequency pump-probe spectroscopy were also reported recently.[33,34]

In this paper, we apply dual-frequency 2D IR spectroscopy to measure the response of two vibrational modes in a conjugated double bond system and investigate whether there is any frequency correlation between them that is caused by valence bond resonances. A good compound for this purpose is ethyl diazoacetate (EDA). Two dominant resonant structures are shown in Fig. 1. We focus on two vibrational modes: the ester C=O and the diazo N=N stretching modes which are separated by one single bond and one double bond. The C=O mode is a double bond in the structure I and becomes a single bond in II, whereas the N=N mode is a double bond in I and a triple bond in II. If solvent or structural fluctuations induce electron clouds in EDA to change between I and II, the bond length and, hence, the frequencies of the two modes are expected to change in an anticorrelated way. Dual-frequency 2D IR spectroscopy can reveal whether this prediction is borne out. In addition, measurements of three-pulse IR photon echo signals and single-color 2D IR spectra were carried out to probe frequency fluctuations of each mode separately. Comparisons of their magnitude and timescale might be useful to get insight into physical origins of the frequency correlation.

We also examine whether multiple conformations of EDA are present and how they affect the 2D IR spectra. In a previous study, Kaplan and Meloy measured temperature dependence of methine proton NMR spectra and suggested that diazoacetic esters, such as EDA, exist in $CDCl_3$ as an equilibrium mixture of the *cis* and *trans* forms in nearly equal amounts.[36] Although vibrational frequency is a useful marker for distinguishing different molecular conformations,[23] previous linear IR studies of EDA did not report observation of spectral features associated with two conformations.[37,38] One possible reason is that the difference in the resonant frequencies of two isomers is less than the linear IR line width and thus they are not resolved. Even under this situation, 2D IR spectroscopy can allow us to find new spectral features by spreading the featureless spectrum into two frequency axes. Here, we will show that 2D IR, especially with the nonrephasing pulse sequence, has a much higher resolving power. It reveals the existence of two intensity components buried in the single C=O band.

2. Methods

2.1. Linear and Nonlinear IR experiments

All nonlinear IR spectroscopic measurements were carried out with the optical parametric amplifier (OPA) constructed in our lab. The experimental setup has been previously described in detail.[39-41] Three femtosecond IR pulses polarized in the same direction were arranged in boxcar geometry and focused into a sample cell with an off-axis parabolic mirror. The time interval between pulse a (with a wavevector $\boldsymbol{k}_a$) and pulse b ($\boldsymbol{k}_b$) was defined as τ and the sign of τ is positive when pulse a preceded pulse b. The delay between the $\boldsymbol{k}_a$ ($\boldsymbol{k}_b$) pulse and pulse c ($\boldsymbol{k}_c$) was defined as the waiting time T for positive (negative) τ. The zero origins of τ and T were determined by monitoring the nonresonant response of neat solvent. In integrated three-pulse photon echo measurements, third-order nonlinear signals in the phase matching direction of $-\boldsymbol{k}_a+\boldsymbol{k}_b+\boldsymbol{k}_c$ were detected by a single element MCT detector and the time-integrated intensities were recorded with scanning τ at T = 300, 500, 750, 1000, 1500, 2000, 3000, and 5000 fs. Single-frequency 2D IR spectra were collected by spectral interferometry measurements. The nonlinear signal was collinearly combined with a local oscillator (LO) field that preceded pulse c by 700 fs, and detected by a 64-element MCT array detector after being dispersed with a spectrograph. The coherence time τ was scanned from –1.96 ps to 1.96 ps with a time step of 7 fs to collect rephasing (R) and nonrephasing (NR) spectra of the ester C=O stretching mode. For the diazo N=N stretching mode, the scan range was set from –2.40 ps to 2.80 ps. The phase of 2D absorptive spectra was retrieved based on IR pump-probe spectra and the projection-slice theorem.[42] Time-resolved pump-probe measurements were also conducted for each mode with parallel and perpendicular polarization to obtain vibrational lifetime and orientational relaxation time.

For the dual-frequency 2D IR experiment, another OPA was built to generate IR pulses tunable in the 3-10 μm range. The whole setup, including the two OPAs and the 2D IR spectrometer, was completely enclosed and purged with dried air. The peak wavelengths of $\boldsymbol{k}_a$ and $\boldsymbol{k}_b$ pulses were tuned to 5.91 μm (1692 cm^{-1}) and those of $\boldsymbol{k}_c$ and LO pulses were set to 4.73 μm (2114 cm^{-1}). The three incident IR beams were arranged in a trapezoid configuration to fulfill the phase matching condition.[22] The experiments were conducted with parallel polarization. The acquisition and process of dual-frequency 2D IR data were performed in the same way as described for the single-frequency 2D IR experiment above. The coherence time τ was scanned from –1.50 ps to 1.50 ps with a time step of 7 fs with a fixed T = 250 fs.

EDA was dissolved in CH_2Cl_2 to a concentration about 8 mM. The solution was filled into a CaF_2 sample cell with a spacer thickness of 250 μm. Linear spectra were recorded with a FT-IR spectrometer with 4-cm^{-1} resolution. The ester C=O mode and diazo N=N mode had an optical density of about 0.20 and 0.27, respectively, after subtraction of the solvent background from the sample spectrum. All measurements were conducted at ambient temperature (20 ± 1 ºC).

2.2. *Simulation*

We simulated the linear and 2D IR spectra using the theoretical formalism based on response functions.[43,44] The finite pulse width effects were taken into account by numerically calculating a triple integral over the electric fields of three excitation pulses.

Detailed computation protocols for simulating the response of a single vibrational mode have already been described in literature.[2,24,25] A key component is the frequency-frequency correlation function (FFCF), $C(t)$, defined as

$$C(t) = \langle \delta\omega(0)\delta\omega(t) \rangle \quad (1)$$

where $\delta\omega(t)$ is the frequency deviation from the average value at time *t*. To describe the dynamical property of individual vibrators, FFCF in the form of a single exponential decay or double exponential decays are often used. Here we utilized a double exponential form with fluctuation amplitudes (Δ_1, Δ_2) and correlation times (τ_1, τ_2) to simulate the results of single color experiments:

$$C(t) = \Delta_1^2 e^{-t/\tau_1} + \Delta_2^2 e^{-t/\tau_2} \quad (2)$$

This form allowed two time scales for the spectral diffusion process and provided a much better fit to the experimental data than the single exponential form.

To describe the vibrational response in dual-frequency 2D IR experiments, all studies thus far have only employed Bloch dynamics.[18,19,22] It is, however, not always valid that the frequency fluctuations can be separated into the fast and static timescales, hence, more general treatment will be useful. When the three incoming pulses are well separated, only two response functions should be considered in each of the R (eq 3) and NR (eq 4) pulse sequences,[2,3,16,43,44]

$$R_{\mathrm{R}}(t_1,t_2,t_3) = |\mu_i|^2|\mu_j|^2 e^{i\omega_i t_1 - i\omega_j t_3} e^{-t_1/2T_{1,i}} e^{-t_2/T_{1,i}} e^{-t_3/2T_{1,j}} \left(1 - e^{i\Delta_{ij} t_3 - t_3/2T_{1,ij}}\right) \exp[-g_i(t_1) + g_{ij}(t_2) - g_j(t_3) - g_{ij}(t_1+t_2) - g_{ij}(t_2+t_3) + g_{ij}(t_1+t_2+t_3)] \quad (3)$$

$$R_{\mathrm{NR}}(t_1,t_2,t_3) = |\mu_i|^2|\mu_j|^2 e^{-i\omega_i t_1 - i\omega_j t_3} e^{-t_1/2T_{1,i}} e^{-t_2/T_{1,i}} e^{-t_3/2T_{1,j}} \left(1 - e^{i\Delta_{ij} t_3 - t_3/2T_{1,ij}}\right) \exp[-g_i(t_1) - g_{ij}(t_2) - g_j(t_3) + g_{ij}(t_1+t_2) + g_{ij}(t_2+t_3) - g_{ij}(t_1+t_2+t_3)] \quad (4)$$

where the time arguments t_1, t_2, and t_3 represent intervals between the light-matter interactions. In eqs 3 and 4, ω_p and μ_p are the fundamental frequency and the transition dipole momentum of mode *p* (*p* = *i* or *j*),

respectively, and Δ_{ij} is the cross anharmonicity between the two modes. The fundamental state of mode p has a lifetime of $T_{1,p}$, and $T_{1,ij}$ is that of the combination state. The line shape functions $g_p(t)$ and $g_{ij}(t)$ are described as $g_p(t) = \int_0^t dt' \int_0^{t'} dt'' C_p(t'')$ and $g_{ij}(t) = \int_0^t dt' \int_0^{t'} dt'' C_{ij}(t'')$, where $C_p(t) = \langle \delta\omega_p(0)\delta\omega_p(t) \rangle$ is the auto FFCF defined by frequency fluctuations of the mode p only and $C_{ij}(t) = \langle \delta\omega_i(0)\delta\omega_j(t) \rangle$ is the cross FFCF which relates fluctuations of the two different modes i and j. The latter includes a correlation factor, f, defined as $f = \langle \delta\omega_i \delta\omega_j \rangle / \sigma_i \sigma_j$ where $\delta\omega_i$ is the frequency shift of mode i and σ_i is the standard deviation of the static frequency distribution. The value of f ranges between –1 and 1, and it describes the degree of the frequency correlation, that is from fully correlated (f = 1) to anticorrelated (f = –1), and uncorrelated (f = 0).[16,17,45] For example, a single exponential function multiplied by f was used as $C_{ij}(t)$ in the model calculations of four-wave mixing signals [45,46] and in the simulation of 2D IR spectra of dicarbonylacetylacetonato rhodium (I) (RDC).[17] The response functions in eqs 3 and 4 were derived under the assumptions that the fluctuation of Δ_{ij} is negligible and transition dipole moments between the fundamental and combination states are equal to those between the ground and fundamental states, that is, $\mu_{ij,i} = \mu_j$, in the weak-coupling limit. Since the FFCF $C_p(t)$ for individual vibrational mode can be determined from measurement and simulation of single color experiments, the remaining terms to be determined in the simulation of dual-frequency 2D IR spectrum are Δ_{ij} and $C_{ij}(t)$. It can be easily checked that when the Bloch approximation of $C_p(t)$ and $C_{ij}(t)$ is employed, the response functions above become the same as those used in the previous works under the assumption of $T_{1,ij}^{-1} = T_{1,i}^{-1} + T_{1,j}^{-1}$.[16,18,19,22]

2.3. DFT calculation

We performed DFT normal mode analysis at B3LYP/6-311++G(d,p) level using Gaussian09 package,[47] and obtained fundamental frequencies and infrared intensities of the N=N and C=O stretching modes for the *cis* and *trans* conformations of EDA. Tomasi's polarizable continuum model[48] was employed to include the solvation effects on these vibrational properties.

3. Results

3.1. FT-IR spectrum

Fig. 2a shows the FT IR spectrum of the EDA/CH_2Cl_2 solution in the frequency range between 1600 and 2200 cm^{-1}. Only two strong bands are observed in this region: the ester C=O stretching band at 1692 cm^{-1} with the FWHM of 28 cm^{-1} (Fig. 2b, solid) and the diazo N=N stretching band at 2114 cm^{-1} with the FWHM of 18 cm^{-1} (Fig. 2c, solid). These peak frequencies are in agreement with those reported for the same molecule in other nonpolar solvents to within a few wavenumbers.[37,38]

3.2. Single-frequency 2D IR spectra

Fig. 3a and b plot the integrated three-pulse photon echo signal intensities of the ester C=O stretching and the diazo N=N stretching mode, respectively, measured at different waiting times. For both modes, the intensity profile is asymmetric along τ at smaller *T* and it becomes more symmetric at longer *T*. The asymmetry is more noticeable for the C=O stretching mode.

Fig. 4 shows 2D IR absorptive spectra of the C=O and the N=N stretching modes measured at *T* = 300, 1000 and 2000 fs. The positive and negative peaks of the C=O mode are more elongated along the diagonal at *T* = 300 fs, and the nodal line between the positive and negative peaks becomes more parallel to the ω_τ axis with increasing *T*. A similar trend is observed in the N=N mode, but the spectral shapes are quite different from those of the C=O mode.

The 2D absorptive spectra in Fig. 4 appear to suggest that the C=O and N=N bands measured in the FT IR spectrum contain a single component. However, it has been shown that 2D IR spectra measured with the NR pulse sequence exhibit higher resolving power for closely spaced spectral features due to the interference effect.[16,39,49] In Fig. 5, we plotted the absolute magnitude 2D IR NR spectra (Fig. 5a and d) and their intensities sliced along the diagonal line (Fig. 5c and f). It is now clear that the spectral profile of the C=O stretching mode consisted of two intensity components, while the 2D IR peak of the N=N mode looks still single. In the presence of spectral inhomogeneity, the diagonal peak in the R spectrum has larger amplitude than that in the NR spectrum, hence, the useful NR peak patterns are less prominent in the phase adjusted absorptive spectrum, which is acquired by adding the R and NR spectra together.

The two components shown in Fig. 5a and 5c indicate the presence of two conformations that are very close in their C=O frequencies, but not resolvable in their N=N frequencies even with 2D IR. This observation is consistent with the results from our DFT calculation that show a small difference in the normal mode frequencies of the *cis* and *trans* conformations. The unscaled frequencies of the N=N and C=O stretching modes are 2211 and 1695 cm^{-1} for the *cis* conformer, and 2205 and 1699 cm^{-1} for the *trans* conformer; their frequency differences (*trans* – *cis*) are –6 cm^{-1} and 4 cm^{-1}, respectively. This small difference is also consistent with the fact that neither the N=N nor C=O mode exhibits a clear doublet in

the FT IR spectrum. The ratio of transition dipole moment $|\mu_{trans}|$: $|\mu_{cis}|$ was calculated to be 1.0:0.44 for the C=O mode and 1.0:1.0 for the N=N mode. These calculated values are presented in Table 1.

Table 2 shows calculated Wiberg bond indices[50,51] of EDA. Wiberg bond indices are similar to classical bond valences. For example, the values for single bonds are close to 1 and for double bonds are close to 2. The calculated values are almost the same for the *cis* and *trans* conformations. The index of C=O bond indicates that it has a mixed single and double bond character, as depicted by the resonance structures in Fig. 1. The mixed bond character of the C-C(=O), C=N and N=N bonds are also consistent with what is predicted from the delocalization of conjugated π-electrons.

We simultaneously simulated the linear IR spectrum (Fig. 2b and c), the integrated photon echo signals (Fig. 3), the 2D IR absorptive spectra (Fig. 4), and the absolute magnitude NR spectra (Fig. 5). We achieved good agreement with the measured results. Table 1 summarizes the auto FFCF parameters and diagonal anharmonicities Δ determined from the simulation as well as the experimental lifetime (T_1) and orientational diffusion constant (D_{OR}) obtained from the polarization dependent IR pump-probe measurements. The simulation included two components for the C=O and N=N modes with the population ratio acquired by the previous NMR study (*trans*:*cis* = 0.46:0.54)[36]. The ratios of transition dipole moment between the two conformers were varied as a fitting parameter in the simulation. We could not well simulate our experimental results when the ratios were fixed to those values obtained from the DFT calculation. We also applied different scaling factors to the DFT calculated C=O and N=N frequencies in the simulation because a single frequency scaling factor could not reproduce the experimental results. The factors for the C=O mode in *trans* and *cis* conformations are 0.9982 and 0.9965, respectively, very close to 1, and those for the N=N mode in *trans* and *cis* conformations are 0.9583 and 0.9570. Given that the *cis* and *trans* conformations are predicted to have very similar vibrational properties (Tables 1 and 2), we assumed that the two conformers have the same auto FFCF. The spectrum calculation was based on the auto FFCFs determined from the integrated photon echo data. It should be pointed out that the frequency separation of the N=N mode in two conformers obtained from the simulation is, at most, 3 cm^{-1} and might be smaller than this value. This is consistent with the result that the observed 2D IR NR spectrum did not clearly show any additional peaks.

3.3. Dual-frequency 2D IR spectrum

Fig. 6a shows the measured dual-frequency 2D IR absorptive spectrum of EDA. The phase adjustment was reasonable, as determined from a comparison between the projection of the 2D spectrum and the dispersed pump-probe signal. Because the frequency separation between the C=O and N=N modes (~420 cm^{-1}) was much larger than the spectral width of the IR pulses, in the experiments we did

not detect any diagonal peaks, for example, at (ω_τ, ω_t) ~ (2114, 2114) cm^{-1} (Fig. 2a). It is clear from Fig. 6a that both positive and negative peaks, as well as the nodal line (green), tilt along the anti-diagonal direction. This tilt indicates that the frequency fluctuations of the two modes are anticorrelated, as discussed below. Moreover, the absolute magnitude of the cross-peak is 1.3 ± 0.1 times stronger in the NR spectrum than in the R spectrum based on three separate measurements. This I_{NR}/I_R intensity ratio is sensitive to the sign of correlation coefficient. A ratio greater than unity indicates a negative correlation between the C=O and N=N modes.

Assuming that the *cis* and *trans* conformations have the same cross FFCFs, we simulated the dual-frequency 2D IR spectrum with several different cross FFCFs: (i) $C_{ij}(t) = f\Delta_c^2 e^{-t/\tau_c}$; (ii) $C_{ij}(t) = fC_{C=O}(t)$, where $C_{C=O}(t)$ is the experimentally determined auto FFCF for the C=O mode based on the photon echo data; (iii) $C_{ij}(t) = fC_{N=N}(t)$, where $C_{N=N}(t)$ is the experimental auto FFCF of the N=N mode. In each case, the off-diagonal anharmonicity Δ_{ij} was adjusted based on the peak separation of positive and negative peaks, and the same value 16 cm^{-1} gave good agreement for all cases. The parameter f was adjusted based on the tilt of the nodal line. Figures 6b and 6c are the simulated spectra obtained from a single exponential cross-FFCF. The best fit parameters are Δ_c = 0.002 fs^{-1}, τ_c = 3000 fs, and f = –0.37 (Fig. 6c). The I_{NR}/I_R ratio from the simulation is 1.8. When f is set to zero, the nodal line of the absorptive spectrum is still slightly tilted along the anti-diagonal direction (Fig. 6b) because the *cis* conformer has a higher C=O frequency and a lower N=N frequency than the *trans* conformer (Table 1). This effect indicates that one has to be careful in interpreting the tilt of nodal line in the presence of multiple isomers. For comparison, we also simulated the spectrum using the Bloch approximation, $C_{ij}(t) = f\{\delta(t)\Gamma_{ij} + \sigma_{ij}^2\}$. The parameters were determined as $\Gamma_{ij}/\pi c$ = 15 cm^{-1}, σ_{ij} = 1.5 ps^{-1}, and f = –0.49 (spectrum not shown). When the cross FFCF was set to be the auto FFCF of the C=O mode with f = –0.85, a very similar spectral pattern was obtained (Fig. 6d). However, when the cross FFCF was set to be the auto FFCF of the N=N mode (Fig. 6e), the tilt of the nodal line cannot be reproduced. To discuss the tilting quantitatively, we define the tilting angle θ as the angle between the ω_τ axis and the nodal line between the positive and negative peaks. The sign of θ is positive when the nodal line declines towards the diagonal (See Fig. 7), and negative when the nodal line declines towards the anti-diagonal. The spectrum in Fig. 6e was simulated with f = –1, but the tilting angle (θ = –12°) is still not quite as negative as the experimental value (–16°), even though f already reaches its negative limit. These results indicate that an accurate determination of f requires correct modeling of the cross FFCF.

3.4. Effects of cross FFCF on the dual frequency 2D IR spectrum

It is useful to check how the slope of the nodal line depends on the cross-peak shape and whether a quantitative relationship between *f* and the slope exists. Figure 7 shows simulated dual-frequency 2D IR absorptive spectra with different correlation factors and the same single exponential frequency correlation function for $C_p(t)$ and $C_{ij}(t)$, that is, $C_p(t) = \Delta_c^2 \exp(-t/\tau_c)$ and $C_{ij}(t) = f\Delta_c^2 \exp(-t/\tau_c)$. In the slow modulation limit ($\Delta_c\tau_c$ = 10, top), the spectral shape significantly depends on *f*. The peaks get greatly elongated along (anti-)diagonal for fully (anti-)correlated frequency fluctuations. It is estimated that $\tan\theta$ = 0.81 and –0.81 for *f* = 1 and –1, respectively when $\Delta_c\tau_c$ = 10. The elongation disappears and peak pattern becomes symmetry along ω_t for the case of no correlation, *f* = 0, and hence $\tan\theta$ = 0. For $\Delta_c\tau_c$ = 1 (middle), this trend is still seen although the overall spectral shapes are quite different from those for $\Delta_c\tau_c$ = 10. The degree of peak tilting ($\tan\theta$ = ± 0.27) is not as much as that for the slow modulation limit.

In the fast modulation limit ($\Delta_c\tau_c$ = 0.1, Fig. 7 bottom), the simulated 2D spectra are independent of *f* and the peak tilting cannot be observed, even for *f* = ± 1. This behavior is easily understandable from the theoretical formalism with response functions. For example, in the response functions for the R pulse sequence, there are four line shape functions dictated by $g_{ij}(t)$ with different time arguments. The line shape function becomes linearly proportional to time in the fast modulation limit ($\Delta_c\tau_c$ «1) and all four line shape functions are completely cancelled out. This is also the case for the NR pulse sequence. Therefore, the 2D IR absorptive spectrum composed of the sum of R and NR responses depend on only frequency correlation function of each vibrational mode, and *f* has no effect on the spectral pattern, as simulated in Fig. 7. When the cross frequency fluctuations are in the homogeneous limit, this consideration is correct. A set of simulated 2D spectra with different correlation functions for $C_p(t)$ and $C_{ij}(t)$ is shown in the top row of Fig. 8. Here, $C_{ij}(t)$ is in the homogeneous limit and $C_p(t)$ is in the inhomogeneous limit. As we discussed above, the spectra simulated with *f* = ± 1 do not exhibit tilting and they are the same as that calculated with *f* = 0. Once the frequency memory between different two modes does not decay quickly, the correlation factor affects the 2D spectral shape regardless of whether $C_p(t)$ and $C_{ij}(t)$ are same or not. One example is plotted in the bottom row of Fig. 8, where $C_p(t)$ is in the slow modulation limit and $C_{ij}(t)$ is in the intermediate range. Tilted spectral patterns are obtained for correlated or anticorrelated vibrators with $\tan\theta$ = ± 0.18 (*f* = ± 1). It should be emphasized that the amount of spectral tilting is determined not only by *f* but also by the cross FFCFs.

Although we assumed the Kubo form for $C_p(t)$ and $C_{ij}(t)$, several important conclusions can be drawn. No tilting of dual-frequency 2D absorptive spectrum indicates either the frequencies of two modes

are uncorrelated or their correlation is quickly lost. In other words, if the peaks are tilted, there should be physical mechanisms which cause intermediate or slow frequency fluctuations in a correlated or anticorrelated way for the two modes. The tilting direction, along diagonal or anti-diagonal, is unambiguously determined by the sign of f and the cross FFCFs do not influence it. The relationship between the correlation factor and tilting of cross-peaks were considered under the Bloch approximation in the past.[3,16,18] Similar calculation results were also reported for the case of a Brownian oscillator bath.[45]

4. Discussion

The most interesting result in this study is that the cross-peak between the ester C=O and diazo N=N modes inclined to the anti-diagonal, indicating the presence of anticorrelated frequency fluctuations. The fluctuations do not have to be in the static distribution limit, but it is certainly not in the fast modulation limit. In the case of EDA, the existence of two different resonance structures shown in Fig. 1 is likely to be one of the reasons to cause the anticorrelation. In a previous study of NMA, the amide-I/II cross-peak was observed to tilt toward the anti-diagonal and the simulation using Bloch approximation gave a negative correlation factor (f = –0.28). It was concluded that the anticorrelated frequency distributions were presumably induced by two dominant valence-bond structures of NMA.[18] Since the anticorrelated frequency fluctuations observed in both systems can be attributed to the presence of resonance structures, it is interesting to check whether there is a relationship between the magnitude of f and the properties of the chemical bonds that are influenced by the resonance. The distance between the C=O and N=N modes of EDA is larger than that between the amide-I (C=O) and the amide-II (C–N) modes in the peptide unit of NMA. Our model calculation suggests that determination of f depends on the cross FFCF of the two vibrators and it needs to be considered when comparisons of f are made. If we assume complete separation of the fast and slow fluctuations in the cross FFCF, the C=O and N=N frequencies are more strongly anticorrelated (f = –0.49) than the amide-I and II modes of NMA, suggesting that the physical distance is not the main factor that determines the magnitude of f.

Another interesting comparison between EDA and NMA is the relative contribution of the two resonance structures. For NMA, the dominant valence-bond structures are neutral and zwitterionic forms where the former has a C–N single bond and the latter has a C=N double bond. The contribution of the neutral form is expected to be much higher than the zwitterionic form. In fact, this bond has an index of 1.19,[52] much closer to a single bond than a double bond. For EDA, both resonant structures in Fig. 1 are zwitterionic. The charge separation in structure I is over a smaller distance than that in structure II. Structure I is expected to have a higher contribution than structure II. Indeed, Table 2 shows that C−C(=O) bond index is 1.1, very close to a single bond, suggesting that structure I dominates. However,

this picture seems inconsistent with the result that the C=O bond index is 1.64, which would suggest a more equal contribution of the two resonant structures. We can reconcile the apparent discrepancy by estimating the bond order from the C=O vibrational frequency. Previous theoretical studies have shown that vibrational force constant, hence, the square of the frequency, is a linear function of the bond order.[53,54] Consider structures I and II as two reference points. We assume that the C-O group in structure II has a typical frequency of 1240 cm^{-1}[55] and a bond order of 1, whereas the C=O group in structure I has a frequency of 1730 cm^{-1} [56] and a bond order equal to the Wiberg bond index of 1.71, calculated for the carbonyl in ethyl acetate. The latter assumption arises from the fact that an ester carbonyl is known to have resonance structures that decrease the C=O bond order to be less than 2. Based on these assumptions and the measured frequency of 1692 cm^{-1}, we estimated the C=O bond order of EDA to be 1.65, in agreement with the calculated bond index. The estimated C=O bond order suggests that structure I is the major resonance structure in EDA.

The FFCFs of the C=O and N=N modes determined based on the *T* dependence of the integrated IR photon echo intensity are different in their amplitudes and time scales of fluctuations. It is conceivable that two vibrational modes, even in the same molecule, have a different solvent shell, hence, different fluctuation dynamics.[57] In our case, the experimental results including the linear IR spectra were reasonably reproduced by the FFCFs with two decaying components in Table 1. The smaller time constants are less than 100 fs, and the product $\Delta_1\tau_1$ of the C=O and N=N modes is 0.095 and 0.20, respectively, indicating these components give rise to a motional narrowing contribution to the line width. The calculated width ($\Delta_1^2\tau_1/\pi c$) is 9.6 cm^{-1} and 6.9 cm^{-1} for the C=O and N=N mode, respectively. The longer decaying components have picosecond time constants and they are in the slow modulation limit, according to the product $\Delta_2\tau_2$ (3.5 for the C=O and 4.0 for the N=N mode). As shown in the model calculations above, a slower fluctuation in a correlated or anticorrelated way is needed to observe a tilted cross-peak pattern. Therefore, the picosecond decays might be related to the frequency fluctuations due to resonance effects. In a systematic study of the dielectric response conducted recently, rotational correlation time of dichloromethane was estimated to be about 2 ps.[58] The frequency fluctuations of EDA on the picosecond time scale may be induced by the rotational motion of solvent molecules. To more clearly assign the molecular mechanisms which cause the frequency fluctuations, one approach is to measure the solvent dependence of the FFCF, such as how the dynamics changes in hydrogen bonding solvents. Another approach is to investigate how FFCF depends on different types of substitutions on the solute molecule. For example, substituent effects on the N=N mode frequency have been studied for several diazo compounds, and the peak IR wavelengths were interpreted in terms of the relevant resonance structures.[37,38] Diazohydrocarbons, such as CH_3CHN_2, are good candidates for future

studies because they have no available resonant structures and are expected to exhibit different FFCF decaying components compared to EDA.

It is desirable to measure dual frequency 2D IR spectra as a function of the waiting time to determine the cross FFCF more accurately. This posted a technical challenge for us in this study because the dispersed pump-probe signal was too weak to allow proper phase adjustment at large *T*. To this end, it would be advantageous to adopt a collinear pulse pair pump-probe geometry so that phasing is automatically achieved.[34,59] It would also be useful to retain the capability of measuring R and NR spectra individually because the NR spectrum can reveal closely spaced spectral features as we demonstrated here. Pulse shaping with phase cycling can achieve both, and therefore should find nice application in future dual-frequency 2D IR studies.

Finally, let's make some remarks on the two isomers of EDA. Although the FT IR spectrum exhibited single bands for the C=O and the N=N modes, our experiment and simulation indicate the existence of two molecular species. The frequency difference between the two species is very small compared with the FWHM for each mode. This is why the peaks in the linear IR spectrum look single. Considering the results of DFT normal mode analysis, we attribute the two species to the *cis* and *trans* isomers. Kaplan and Meloy computed the free energies of activation from *cis* to *trans* and from *trans* to *cis* forms to be 13.3 and 13.2 kcal/mol, respectively, at 298 K, and the rates of interconversion were 971 s^{-1} (*cis* → *trans*) and 1222 s^{-1} (*trans* → *cis*).[36] The rotational isomerization processes around a C–C bond that exhibits partial double bond character are very slow in comparison with the time resolution of 2D IR spectroscopy, hence, the IR spectral features are observed as an ensemble average of these two structural isomers.

5. Conclusions

We studied the frequency fluctuations and correlation of the ester C=O and diazo N=N stretching modes in a conjugated system by third-order nonlinear IR spectroscopy. The dual-frequency 2D IR spectrum exhibits an anti-diagonally tilted cross-peak of the two modes. The degree of tilting cannot be explained solely by the presence of *cis* and *trans* conformers. This clearly indicates that the frequency fluctuations of the two modes are anticorrelated. Most likely, this anticorrelation originates from concerted change in bond orders when the contributions represented by different resonant structures vary. Our theoretical calculation shows that no cross-peak titling would be present if there was no correlation or the frequency fluctuations were in the fast modulation limit. The observed anticorrelation, therefore, suggests that the cross FFCF of the two modes has a static and/or a slowly decaying components. Indeed, our simulation using a single exponential cross FFCF gives $\Delta_c \tau_c = 6$, which is in the slow modulation

limit. The corresponding τ_c = 3 ps is on a time scale similar to the solvent rotational correlation time, indicating that the possible role of solvent fluctuations in inducing the observed anticorrelation.

Acknowledgements. This research was supported by grants from the US National Science Foundation (CHE-0450045, CHE-0802913, and CHE-1013071). The DFT calculation was performed with the aid of the computational modeling facility funded by NSF (CHE-0840513).

References

[1] M.C. Asplund, M.T. Zanni, R.M. Hochstrasser, Proc. Natl. Acad. Sci. U.S.A. 97 (2000) 8219.

[2] R.M. Hochstrasser, Adv. Chem. Phys. 132 (2006) 1.

[3] M. Khalil, N. Demirdöven, A. Tokmakoff, J. Phys. Chem. A 107 (2003) 5258.

[4] M. Cho, Chem. Rev. 108 (2008) 1331.

[5] W. Zhuang, T. Hayashi, S. Mukamel, Angew. Chem. Int. Ed. 48 (2009) 3750.

[6] S.-H. Shim, M.T. Zanni, Phys. Chem. Chem. Phys. 11 (2009) 748.

[7] M.D. Fayer, Annu. Rev. Phys. Chem. 60 (2009) 21.

[8] J. Bredenbeck, J. Helbing, C. Kolano, P. Hamm, ChemPhysChem 8 (2007) 1747.

[9] T. Elsaesser, Acc. Chem. Res. 42 (2009) 1220.

[10] Z. Ganim, H.S. Chung, A.W. Smith, L.P. DeFlores, K.C. Jones, A. Tokmakoff, Acc. Chem. Res. 41 (2008) 432.

[11] S. Woutersen, Y. Mu, G. Stock, P. Hamm, Chem. Phys. 266 (2001) 137.

[12] Y.S. Kim, R.M. Hochstrasser, Proc. Natl. Acad. Sci. U.S.A. 102 (2005) 11185.

[13] J. Zheng, K. Kwak, J. Xie, M.D. Fayer, Science 313 (2006) 1951.

[14] J.M. Anna, M.R. Ross, K.J. Kubarych, J. Phys. Chem. A 113 (2009) 6544.

[15] H. Maekawa, N.-H. Ge, J. Phys. Chem. B 116 (2012) 11292.

[16] N.-H. Ge, M.T. Zanni, R.M. Hochstrasser, J. Phys. Chem. A 106 (2002) 962.

[17] N. Demirdoven, M. Khalil, A. Tokmakoff, Phys. Rev. Lett. 89 (2002) 237401.

[18] I.V. Rubtsov, J. Wang, R.M. Hochstrasser, Proc. Natl. Acad. Sci. U.S.A. 100 (2003) 5601.

[19] I.V. Rubtsov, J. Wang, R.M. Hochstrasser, J. Chem. Phys. 118 (2003) 7733.

[20] I.V. Rubtsov, K. Kumar, R.M. Hochstrasser, Chem. Phys. Lett. 402 (2005) 439.

[21] D.V. Kurochkin, S.R.G. Naraharisetty, I.V. Rubtsov, J. Phys. Chem. A 109 (2005) 10799.

[22] S.R.G. Naraharisetty, D.V. Kurochkin, I.V. Rubtsov, Chem. Phys. Lett. 437 (2007) 262.

[23] L.J. Bellamy, The Infra-Red Spectra of Complex Molecules. 2nd ed, John Wiley & Sons, Inc., New York, 1958.

[24] P. Hamm, M. Lim, R.M. Hochstrasser, Phys. Rev. Lett. 81 (1998) 5326.

[25] M.D. Fayer Ed., Ultrafast Infrared and Raman Spectroscopy. Marcel Dekker, New York, 2001.
[26] S. Park, K. Kwak, M. Fayer, Laser Phys. Lett. 4 (2007) 704.
[27] H.J. Bakker, J.L. Skinner, Chem. Rev. 110 (2009) 1498.
[28] K. Ohta, J. Tayama, K. Tominaga, Phys. Chem. Chem. Phys. 14 (2012) 10455.
[29] J. Stenger, D. Madsen, P. Hamm, E.T.J. Nibbering, T. Elsaesser, J. Phys. Chem. A 106 (2002) 2341.
[30] J. Stenger, D. Madsen, J. Dreyer, P. Hamm, E.T.J. Nibbering, T. Elsaesser, Chem. Phys. Lett. 354 (2002) 256.
[31] I. Noda, J. Mol. Struct. 883-884 (2008) 2.
[32] Y. Mee Jung, I. Noda, Appl. Spectrosc. Rev. 41 (2006) 515.
[33] H. Bian, J. Li, X. Wen, Z. Sun, J. Song, W. Zhuang, J. Zheng, J. Phys. Chem. A 115 (2011) 3357.
[34] J. Borek, F. Perakis, F. Kläsi, S. Garrett-Roe, P. Hamm, J. Chem. Phys. 136 (2012) 224503.
[35] I.V. Rubtsov, Acc. Chem. Res. 42 (2009) 1385.
[36] F. Kaplan, G.K. Meloy, J. Am. Chem. Soc. 88 (1966) 950.
[37] P. Yates, B.L. Shapiro, N. Yoda, J. Fugger, J. Am. Chem. Soc. 79 (1957) 5756.
[38] A. Foffani, C. Pecile, S. Ghersetti, Tetrahedron 11 (1960) 285.
[39] H. Maekawa, F. Formaggio, C. Toniolo, N.-H. Ge, J. Am. Chem. Soc. 130 (2008) 6556.
[40] H. Maekawa, M. De Poli, C. Toniolo, N.-H. Ge, J. Am. Chem. Soc. 131 (2009) 2042.
[41] H. Maekawa, M. De Poli, A. Moretto, C. Toniolo, N.-H. Ge, J. Phys. Chem. B 113 (2009) 11775.
[42] D.M. Jonas, Annu. Rev. Phys. Chem. 54 (2003) 425.
[43] S. Mukamel, Principles of nonlinear optical spectroscopy, Oxford University Press, Inc., New York, 1995.
[44] J. Sung, R.J. Silbery, J. Chem. Phys. 115 (2001) 9266.
[45] R. Venkatramani, S. Mukamel, J. Chem. Phys. 117 (2002) 11089.
[46] S. Schmitt-Rink, S. Mukamel, K. Leo, J. Shah, D.S. Chemla, Phys. Rev. A 44 (1991) 2124.
[47] M.J. Frisch, G.W. Trucks, H.B. Schlegel, G.E. Scuseria, M.A. Robb, J.R. Cheeseman, G. Scalmani, V. Barone, B. Mennucci, G.A. Petersson, H. Nakatsuji, M. Caricato, X. Li, H.P. Hratchian, A.F. Izmaylov, J. Bloino, G. Zheng, J.L. Sonnenberg, M. Hada, M. Ehara, K. Toyota, R. Fukuda, J. Hasegawa, M. Ishida, T. Nakajima, Y. Honda, O. Kitao, H. Nakai, T. Vreven, J.A. Montgomery, Jr., J.E. Peralta, F. Ogliaro, M. Bearpark, J.J. Heyd, E. Brothers, K.N. Kudin, V.N. Staroverov, T. Keith, R. Kobayashi, J. Normand, K. Raghavachari, A. Rendell, J.C. Burant, S.S. Iyengar, J. Tomasi, M. Cossi, N. Rega, J.M. Millam, M. Klene, J.E. Knox, J.B. Cross, V. Bakken, C. Adamo, J. Jaramillo, R. Gomperts, R.E. Stratmann, O. Yazyev, A.J. Austin, R. Cammi, C. Pomelli, J.W. Ochterski, R.L. Martin, K. Morokuma, V.G. Zakrzewski, G.A. Voth, P. Salvador,

J.J. Dannenberg, S. Dapprich, A.D. Daniels, O. Farkas, J.B. Foresman, J.V. Ortiz, J. Cioslowski, D.J. Fox, Gaussian 09, Revision C.01. Gussian, Inc., Wallingford, CT, 2010.

[48] J. Tomasi, B. Mennucci, R. Cammi, Chem. Rev. 105 (2005) 2999.

[49] S. Sul, D. Karaiskaj, Y. Jiang, N.-H. Ge, J. Phys. Chem. B 110 (2006) 19891.

[50] K.B. Wiberg, Tetrahedron 24 (1968) 1083.

[51] J.P. Foster, F. Weinhold, J. Am. Chem. Soc. 102 (1980) 7211.

[52] G. Cuevas, V. Renugopalakrishnan, G. Madrid, A.T. Hagler, Phys. Chem. Chem. Phys. 4 (2002) 1490.

[53] A.I. Finkel'shtein, Theor. Exp. Chem. 1 (1965) 178.

[54] H.H. Jensen, Acta Chem. Scand. 23 (1969) 3163.

[55] L.J. Bellamy, The Infra-red Spectra of Complex Molecules, 1954.

[56] K.J. Morgan, N. Unwin, J. Chem. Soc. B (1968) 880.

[57] J.-H. Ha, Y.S. Kim, R. Hochstrasser, M., J. Chem. Phys. 124 (2006) 064508.

[58] J. Hunger, A. Stoppa, A. Thoman, M. Walther, R. Buchner, Chem. Phys. Lett. 471 (2009) 85.

[59] L.P. DeFlores, R.A. Nicodemus, A. Tokmakoff, Opt. Lett. 32 (2007) 2966.

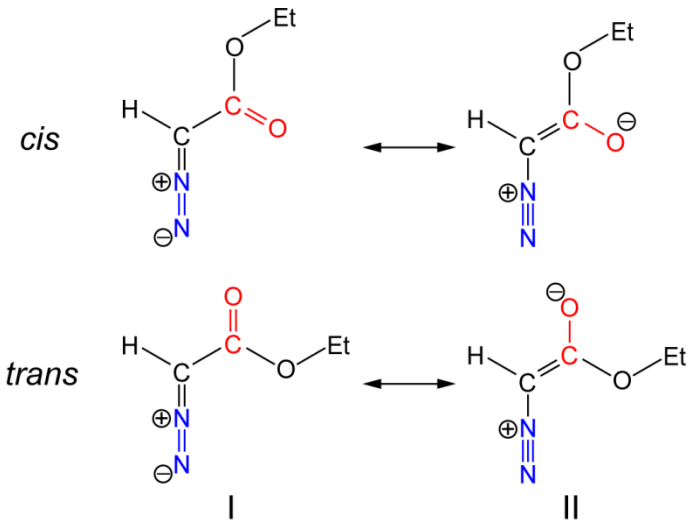

Fig. 1. Resonant structures of *cis* and *trans* ethyl diazoacetate.

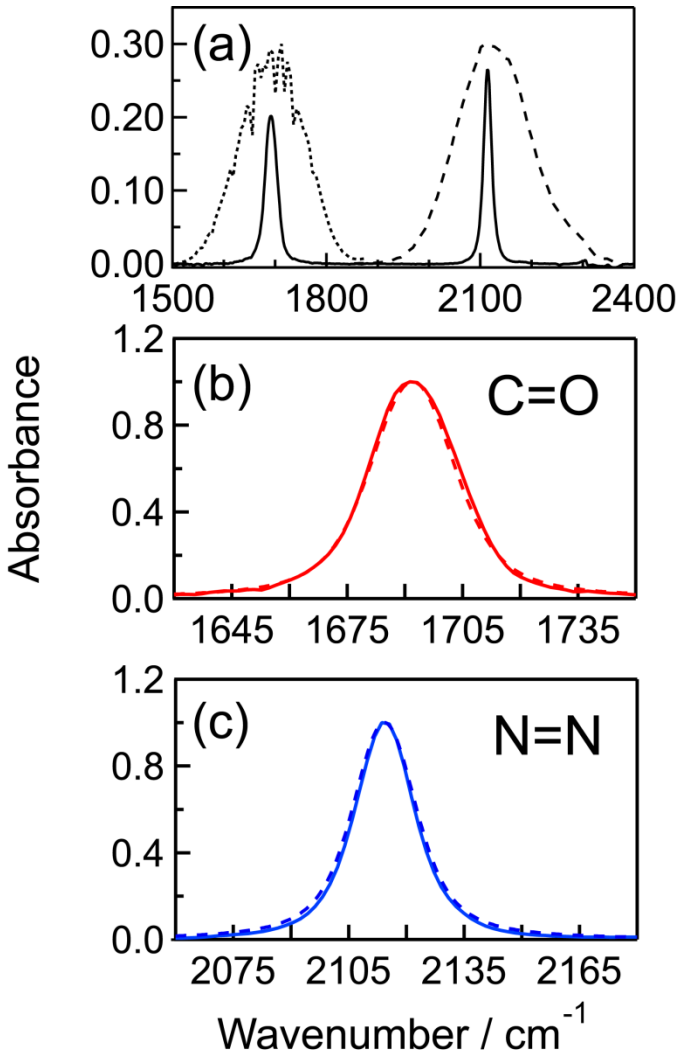

Fig. 2. (a) The FT IR spectrum of ethyl diazoacetate measured in dichloromethane. A solvent background spectrum was subtracted. Infrared pulse spectra to excite the ester C=O mode (dotted line) and the diazo N=N mode (dashed line) are also shown. The measured (solid line) and simulated (dashed line) linear spectra of the ester C=O mode and the diazo N=N mode are plotted in the panel (b) and (c), respectively.

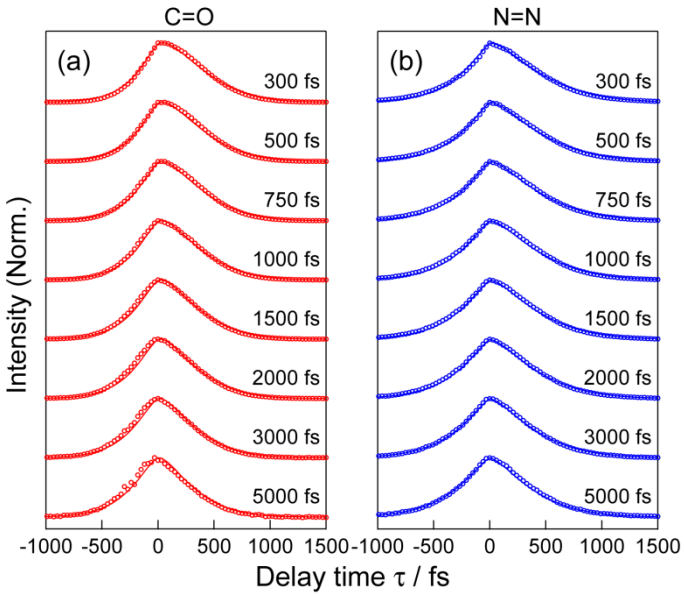

Fig. 3. Measured (circles) and simulated (solid lines) integrated three-pulse IR photon echo signals at different waiting times: the C=O stretching mode (a); the N=N stretching mode (b). The waiting time *T* for each spectrum is indicated above the trace.

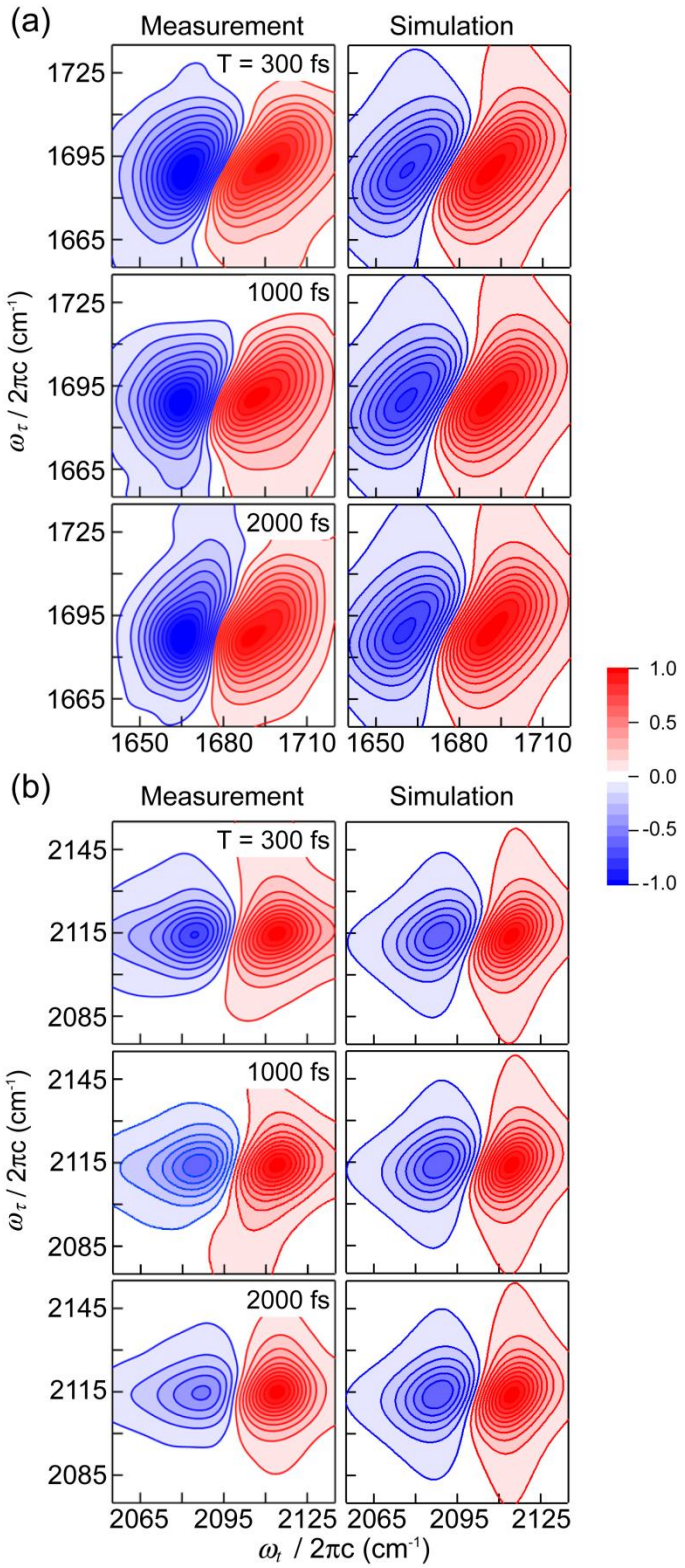
(a)
Measurement
Simulation
T = 300 fs
1000 fs
2000 fs
1725
1695
1665
1650
1680
1710
ω_τ / 2πc (cm^{-1})
(b)
2145
2115
2085
2065
2095
2125
ω_t / 2πc (cm^{-1})
1.0
0.5
0.0
-0.5
-1.0

Fig. 4. Measured (left) and simulated (right) 2D IR absorptive spectra under parallel polarization and with the waiting time of 300, 1000, and 2000 fs from top to bottom: the C=O stretching mode (a); the N=N stretching mode (b). The spectra were normalized by the peak amplitude.

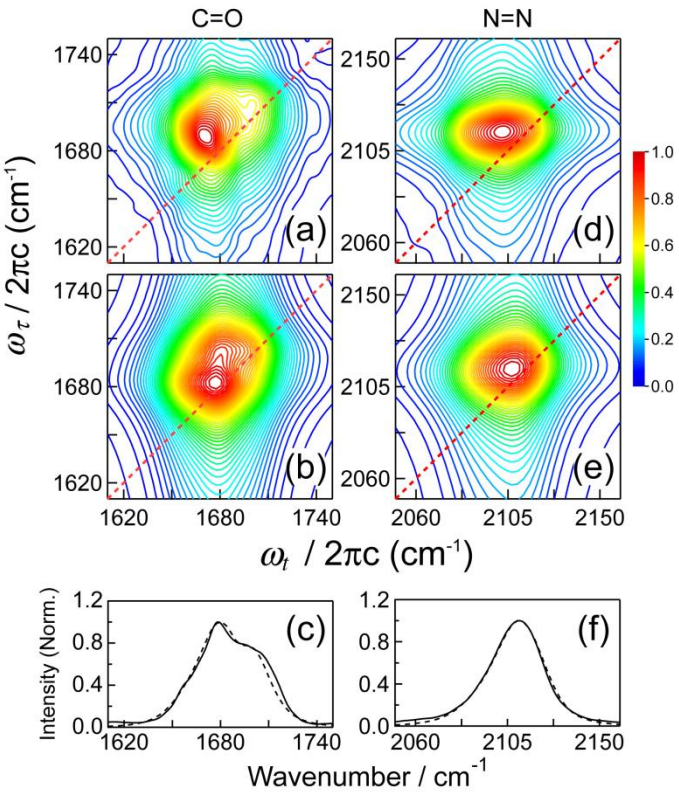

Fig. 5. Absolute magnitude of 2D IR NR spectra at T = 300 fs for the C=O (a, b) and N=N (d, e) stretching modes: measurement (a, d); simulation (b, e). Each spectrum was normalized by the peak intensity and plotted with equally-spaced 40 contour lines between 0 and 1. Measured and simulated 2D IR spectral intensities were sliced along the diagonal line (red dotted line), and showed by solid and dashed lines, respectively, for the C=O (c) and N=N (f) mode.

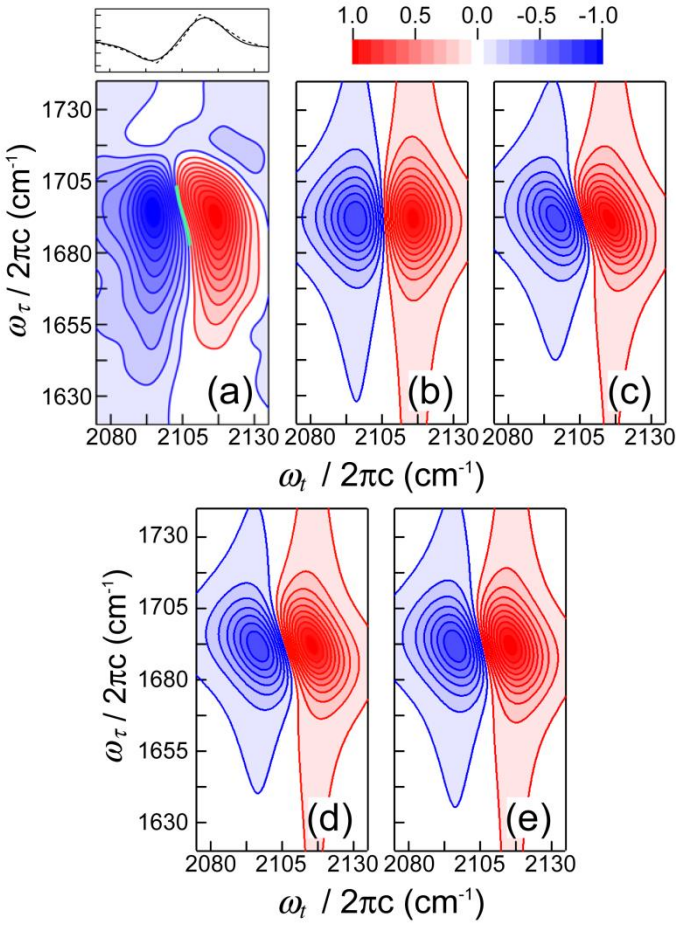

Fig. 6. Dual-frequency 2D absorptive spectra between the C=O and the N=N modes of ethyl diazoacetate in dichloromethane: (a) measurement; (b) simulation under the Bloch approximation and no frequency correlation; (c) simulation under the Bloch approximation for correlated frequency; (d) simulation with the cross FFCF same as the auto FFCF of the C=O mode; (e) simulation with the cross FFCF same as the auto FFCF of the N=N mode. The green line in the panel (a) represents the nodal line between the positive and negative peaks. Projection onto the ω_t axis of the phase-adjusted 2D absorptive spectrum and a dispersed dual-frequency pump-probe spectrum are also shown by solid and dashed lines, respectively, in the panel above (a).

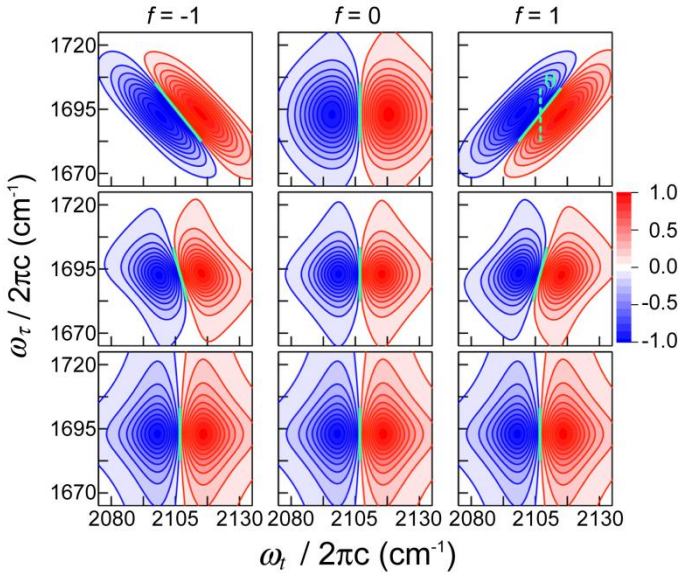

Fig. 7. Simulated dual-frequency 2D IR absorptive spectra with different correlation factors [f = –1 (left); 0 (center); 1 (right)] and the same FFCFs for $C_p(t)$ and $C_{ij}(t)$: Δ_c = 2 ps^{-1} and τ_c = 5 ps (top); Δ_c = 2 ps^{-1} and τ_c = 0.5 ps (middle); Δ_c = 20 ps^{-1} and τ_c = 0.005 ps (bottom). The value of Δ_c in the homogeneous limit is different from the others to get the resultant 2D IR spectral linewidth similar. The green line in each spectrum represents the nodal line between the positive and negative peaks.

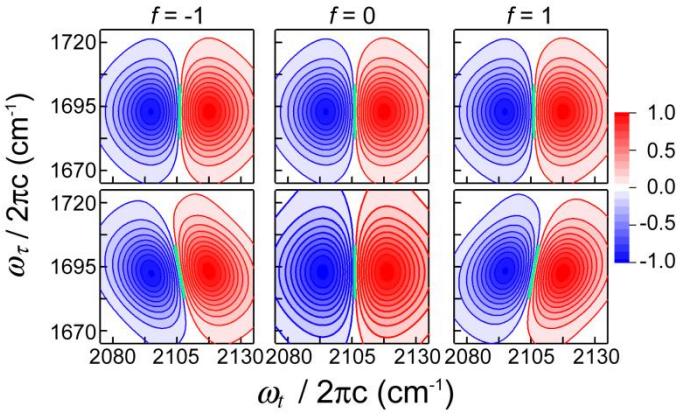

Fig. 8. Simulated dual-frequency 2D IR absorptive spectra with different correlation factors [f = –1 (left); 0 (center); 1 (right)] and different FFCFs for $C_p(t)$ and $C_{ij}(t)$: $\Delta_{c,p}$ = 2 ps^{-1}, $\tau_{c,p}$ = 5 ps, $\Delta_{c,ij}$ = 2 ps^{-1} and $\tau_{c,ij}$ = 0.005 ps (top): $\Delta_{c,p}$ = 2 ps^{-1}, $\tau_{c,p}$ = 5 ps, $\Delta_{c,ij}$ = 2 ps^{-1} and $\tau_{c,ij}$ = 0.5 ps (bottom). The green line in each spectrum represents the nodal line between the positive and negative peaks.

Table 1. Parameters to Simulate the Linear and Nonlinear IR Responses of the Ester C=O and Diazo N=N Stretching Modes.

	Measurement and simulation		DFT calculation	
mode	C=O	N=N	C=O	N=N
$\tilde{\nu}_{peak}$ / cm^{-1}	1692	2114		
$\Delta\tilde{\nu}_{FWHM}$ / cm^{-1}	28	18		
T_1 / ps	1.9 ± 0.1	1.2 ± 0.1		
D_{OR} / 10^{-3} ps^{-1}	31 ± 4	35 ± 4		
$\tilde{\nu}_{trans}$ / cm^{-1}	1696	2113	1699	2205
$\tilde{\nu}_{cis}$ / cm^{-1}	1689	2116	1695	2211
$\lvert\mu_{trans}\rvert$: $\lvert\mu_{cis}\rvert$	1.0:1.2	1.0:0.92	1.0:0.44	1.0:1.0
P_{trans} : P_{cis}	0.46:0.54[a]			
Δ_1 / ps^{-1}	9.5	3.3		
Δ_2 / ps^{-1}	1.4	1.0		
τ_1 / ps	0.010	0.060		
τ_2 / ps	2.5	4.0		
$\Delta_1^2\tau_1/\pi c$/ cm^{-1}	9.6	6.9		
Δ / cm^{-1}	28	25		
Δ_{ij} / cm^{-1}	16			

[a] Ref. [36].

Table 2. Wiberg bond indices of chemical bonds in ethyl diazoacetate.

Bond	*cis*	*trans*
C=O	1.640	1.641
C−C(=O)	1.104	1.097
C=N	1.332	1.331
N=N	2.433	2.424

Table of contents